

pubs.acs.org/JPCA Article

Reduced Scaling Real-Time Coupled Cluster Theory

Published as part of The Journal of Physical Chemistry A virtual special issue "Krishnan Raghavachari Festschrift".

Benjamin G. Peyton, Zhe Wang, and T. Daniel Crawford*



Cite This: J. Phys. Chem. A 2023, 127, 8486-8499



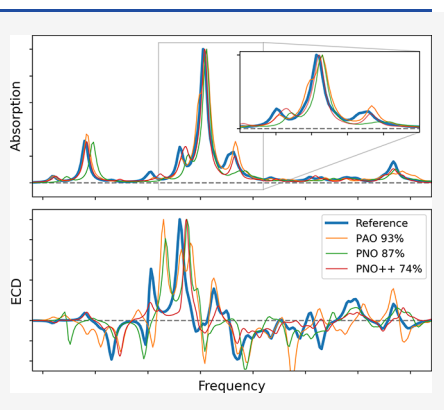
ACCESS I

III Metrics & More

Article Recommendations

s Supporting Information

ABSTRACT: Real-time coupled cluster (CC) methods have several advantages over their frequency-domain counterparts, namely, response and equation of motion CC theories. Broadband spectra, strong fields, and pulse manipulation allow for the simulation of complex spectroscopies that are unreachable using frequency-domain approaches. Due to the high-order polynomial scaling, the required numerical time propagation of the CC residual expressions is a computationally demanding process. This scaling may be reduced by local correlation schemes, which aim to reduce the size of the (virtual) orbital space by truncation according to user-defined parameters. We present the first application of local correlation to real-time CC. As in previous studies of locally correlated frequency-domain CC, traditional local correlation schemes are of limited utility for field-dependent properties; however, a perturbation-aware scheme proves promising. A detailed analysis of the amplitude dynamics suggests that the main challenge is a strong time dependence of the wave function sparsity.



1. INTRODUCTION

Dynamic molecular responses induced by electromagnetic fields give rise to a number of experimental techniques for the detailed investigation and characterization of light-matter interactions and structure, including absorption, circular dichroism (CD), and Raman scattering spectroscopies. Such techniques are essential for modern synthetic chemistry in both research and industrial settings. Theoretical/computational simulations of such spectra have advanced to the point that they are now considered a "full partner with experiment", providing high-quality benchmark data for affirming or predicting many molecular responses, thereby increasing the accuracy and reliability of spectral assignments and molecular structure determination. Computation of spectroscopic properties with current ab initio methods generally involves frequency-domain perturbation theory, commonly referred to as response theory.³

The development of modern response methods covers the broad range of quantum-chemical techniques, including time-dependent Hartree–Fock (TDHF)^{6–9} (also known as the random phase approximation (RPA)⁸), second-order polarization propagator (SOPPA),¹⁰ the algebraic diagrammatic construction (ADC),^{11–13} multiconfigurational self-consistent field (MCSCF) theory,¹⁴ time-dependent density functional theory (TDDFT),¹⁵ Møller–Plesset perturbation theory,^{16,17} and others (see the review by Norman¹⁸ and the text by Norman, Ruud, and Saue¹⁹ for an excellent overview of the many formulations and applications of response theory). Coupled cluster (CC) response theory,^{20,21} in particular, has

emerged as one of the most robust approaches to frequency-domain property calculations. ^{22,23}

There are several drawbacks to the response formalism.^{24–26} First and foremost, the perturbations must be "small" relative to the intramolecular forces present in the system. This immediately precludes the possibility of simulating many experiments such as high-intensity X-ray spectroscopy, which have numerous applications in materials science, for example. Second, response theory typically assumes weak, adiabatically switched-on monochromatic fields. Experimental measurements, on the other hand, can make use of complex, multiphase procedures involving tuned laser pulses, pumpprobe analysis, etc.²⁷ Finally, temporally controlled multiphoton events such as high harmonic generation (HHG)^{28,29} lie outside the realm of the response formalism. Together, these drawbacks mean that a wide variety of experiments cannot be straightforwardly predicted or supplemented with response theory calculations. To overcome this obstacle, it is useful to pursue nonperturbative time-domain electronic structure theory, ^{23,25,26} where there are fewer limitations on the form of the perturbing electromagnatic field.

Received: July 30, 2023 Revised: September 13, 2023 Published: October 2, 2023





Real-time time-dependent density functional theory (RT-TDDFT) was introduced in the 1990s (then called the timedependent local density approximation) 30-33 and provides a cost-effective approach to time-dependent simulations. 25,26,34-39 Efforts to introduce computational savings into RT-TDDFT have largely focused on reducing simulation times, utilizing techniques such as Padé approximants to accelerate the convergence of the Fourier transform³⁸ and fitting schemes to avoid the Fourier transform altogether, thus ameliorating the problem of short trajectories resulting in lowresolution spectra. 40 Repisky et al. introduced the concept of dipole-pair contributions, 41,42 which are typically less complicated than the total electric dipole and thus may be individually approximated efficiently using the techniques mentioned above.³⁸ However, the challenges of frequencydomain DFT carry over directly to the time domain, such as the underestimation of excited-state energies⁴³ and difficulties arising from the adiabatic approximation.^{38,44,45} We refer the reader to a recent comprehensive review article²⁶ and citations therein for a more complete discussion of these challenges. Regardless, the success of RT-TDDFT under most conditions combined with its drastically reduced computational cost makes it the only viable method for large molecules at present.

The alternative of real-time CC (RTCC) methods has been discussed nearly as far back as the origins of CC itself in the realm of nuclear physics. 46-49 More recently, a renewed interest in RTCC has developed for the reasons discussed above, and in the past 10 years several implementations have been reported, 50-55 with new insights into the aspects of numerical integration 53,56 and interpretation 53,57 as well as applications for a number of spectral properties. 52,54,58-60 Orbital-adaptive 1 and orbital-optimized 1 variants have also explored the limitations of unrelaxed canonical Hartree—Fock orbitals as well as the effects of alternative reference orbitals on the propagation of unphysical imaginary components to energetics and electric dipole moments. Notably absent, however, are studies of the ability to reduce the cost of RTCC methods.

Borrowing from the vast literature of reduced-scaling ground-state or frequency-domain CC, there are numerous potential candidates for reducing the cost of RTCC beyond the successful approaches implemented for RT-TDDFT described above. First, the standard nonperturbative truncated approaches used for properties such as CC2⁶² and CC3⁶³ are immediately possible, as are property-optimized basis sets. 64-72 Further, details of implementation such as the choice of intermediate tensors, the effects of single or mixed precision, or the use of graphical processing units have only just begun to be explored. 55,73 An alternative formulation developed separately by the DePrince and Bartlett groups, dubbed the timedependent equation-of-motion CC (TD-EOM-CC) method, 52,54,58-60 reduces the cost by targeting the difficulty of numerical integration of multiple "stiff" coupled differential equations. By selection of a given moment function to propagate in time, the coupled right- and left-hand wave function amplitudes of CC theory do not have to be propagated separately, reducing both the number and difficulty of numerical integrations required.

The principal drawback for RTCC theory, however, is its high-degree polynomial scaling, which further increases the cost of even short propagations in time. For time-independent ground-state CC energy calculations, numerous techniques—referred to as "local correlation" or "reduced-scaling"

methods—have been developed over the last few decades to ameliorate this shortcoming. These methods seek to build a compact virtual-orbital (correlation) space based on lower-cost criteria, such as (pair) energies from low-order perturbation theory or atomic-orbital charge analysis, thereby reducing the exponential cost of the method, possibly as far as linear scaling. While still only routine for ground-state calculations, these methods and variants thereof have shown promise in the calculation of static electric dipole moments as well as selected linear response properties. 72,105–108

In this work, we report the first application of local correlation to RTCC. The effects of occupied- and virtual-space localizations are considered for the simulations of small hydrogen clusters in the presence of electric field perturbations. Absorption cross sections as well as electronic CD (ECD) spectra are computed using successively smaller fractions of the canonical orbital space using the popular projected atomic orbital (PAO)^{76,109–111} and pair natural orbital (PNO)^{87,112} schemes. Additionally, we compare these to the recent perturbed pair natural orbital (PNO++) approach, which has been formulated specifically for computing field-induced properties. The results are analyzed with respect to the full-space simulations. Finally, wave function amplitude dynamics is investigated in order to determine the extent to which these schemes suppress or cause large amplitude deviations, which cause instabilities in numerical integration and spurious oscillations in the dipole trajectory.

2. THEORETICAL BACKGROUND

2.1. Real-Time Coupled Cluster Theory. Conventional RTCC implementations begin by solving the ground-state right- and left-hand CC wave function amplitude (residual) equations in the absence of the external field, *viz.*,

$$\langle \mu | \overline{H} | \Phi \rangle = 0 \tag{1a}$$

$$\langle \Phi | (1 + \hat{\Lambda}) [\overline{H}, \tau_{\mu}] | \Phi \rangle = 0 \tag{1b}$$

where $|\Phi\rangle$ is the Hartree–Fock ground-state determinant, $|\mu\rangle$ are substituted determinants (singles, doubles, *etc.*) obtained by the action of the second-quantized excitation and deexcitation operators τ_{μ} and \bar{H} is the similarity-transformed electronic Hamiltonian,

$$\bar{H} = e^{-\hat{T}} \hat{H} e^{\hat{T}} \tag{2}$$

with right-hand cluster operators

$$\hat{T} = \sum_{\mu}^{N} \hat{T}_{\mu} \tag{3a}$$

$$\hat{T}_{\mu} = \sum_{\mu} \tau_{\mu} t_{\mu} \tag{3b}$$

and left-hand cluster operators

$$\hat{\Lambda} = \sum_{\mu}^{N} \hat{\Lambda}_{\mu} \tag{4a}$$

$$\hat{\Lambda}_{\mu} = \sum_{\mu} \tau_{\mu}^{\dagger} \lambda_{\mu} \tag{4b}$$

The time evolution of the amplitudes is governed by the nonlinear differential equations obtained through the time-dependent Schrödinger equation (in atomic units):

$$i\frac{\mathrm{d}t_{\mu}(t)}{\mathrm{d}t} = \langle \mu | \overline{H}(t) | \Phi \rangle \tag{5a}$$

$$-i\frac{\mathrm{d}\lambda_{\mu}(t)}{\mathrm{d}t} = \langle \Phi | (1 + \hat{\Lambda}(t)) [\overline{H}(t), \tau_{\mu}] | \Phi \rangle \tag{5b}$$

The right-hand sides of eqs 5a and 5b are the same as the residual expressions above, where we have explicitly noted the time dependence of the Hamiltonian and the cluster operators. By including a field perturbation as a time-dependent addition to the Fock operator, the right-hand sides of these equations may be computed by updating the Hamiltonian from time t to time t' = t + h and recomputing the residual expressions. This is achieved using a numerical integrator, which produces solutions to equations of the form

$$\frac{\mathrm{d}y(t)}{\mathrm{d}t} = f(y, t) \tag{6}$$

Here y is a concatenation of the t_{μ} and λ_{μ} vectors, and the function f represents a corresponding concatenation of the residual expressions. Multiple integration schemes are possible, and for simplicity we adopt the popular fourth-order Runge–Kutta integrator, ¹¹³ defined by

$$k_{1} = f(y, t)$$

$$k_{2} = f\left(y + \frac{1}{2}hk_{1}, t + \frac{1}{2}h\right)$$

$$k_{3} = f\left(y + \frac{1}{2}hk_{2}, t + \frac{1}{2}h\right)$$

$$k_{4} = f(y + hk_{3}, t + h)$$
(7)

with time step h, and the propagated tensor is computed as

$$y(t+h) = y(t) + \frac{1}{6}h(k_1 + 2k_2 + 2k_3 + k_4)$$
(8)

2.2. Properties. Within the dipole approximation, the complex time-domain response tensors α (the polarizability tensor) and G' (the optical activity/Rosenfeld tensor) can be defined by low-order expansions of the time-dependent electric and magnetic dipole moment expectation values in an electric field E with frequency ω_1^{-1} viz.,

$$\langle \mu \rangle_i = \mu_0 + \alpha_{ij} E_j \tag{9a}$$

$$\langle m \rangle_i = -\frac{1}{\omega} \frac{\partial E_j}{\partial t} G'_{ij}$$
 (9b)

where i and j are Cartesian coordinates and the notation suppresses the time dependence for clarity. The dipole strength function S is related to the imaginary component of α by

$$S(t) \propto \text{Tr}[\text{Im}(\alpha(t))]$$
 (10)

and Fourier transformation of S to the frequency domain yields the broadband absorption spectrum. The differential molar extinction coefficient is proportional to the imaginary part of the Rosenfeld G' tensor¹¹⁴ by

$$\eta(t) \propto -\text{Tr}[\text{Im}(\mathbf{G}'(t))]$$
(11)

and the Fourier transform of eq 11 yields the ECD spectrum.

We note here two important points. First, we could just as easily define both α and G' with respect to the electric dipole expectation value; however, by expanding both moments in an electric field, we may recover both properties by computing the expectation values of both the electric and magnetic dipole operators along the same electric-field-perturbed trajectory. In principle, we may compute *any* electric-field-perturbed expectation value from a single propagation; this is in contrast to the TD-EOM-CC method, which propagates a single moment function. Additional expectation values would require additional moment function propagations.

Second, we note that the low-order expansions in eq 11 are an approximation. The total dipole moments will contain many higher-order terms; however, at the field strengths used in this work, these effects are expected to be negligible. These terms can be separated and have been examined in the context of real-time simulations of X-ray absorption spectroscopy (XAS).⁶⁰ While very important to the advantages of the RTCC method, these effects are beyond the scope of the current work.

2.3. Local Correlation. 2.3.1. Projected Atomic Orbitals. In the PAO method, the virtual space is localized based on spatial criteria derived from the set of atom-centered atomic orbital (AO) basis functions. The occupied orbitals are first localized using conventional criteria such as those defined by Pipek and Mezey¹¹⁵ or Boys.¹¹⁶ Then the virtual space is obtained by projecting away contributions from the occupied space:

$$\tilde{\mathbf{C}}' = \mathbf{1} - \mathbf{DS} \tag{12}$$

where D is the Hartree–Fock density matrix and S is the overlap matrix (both in the AO basis) and \tilde{C}' is the resulting PAO coefficient matrix, which has the same dimension as the original AO basis. Thus, the PAOs are orthogonal to the occupied space but remain nonorthogonal among themselves.

The reduction of the size of the correlation (virtual) space is achieved by choosing a subset of the PAOs—the virtual "domain"—for each occupied orbital. The selection process is based on an atom-by-atom approach in which all the AO basis functions associated with a given atom are used to compute a "completeness function" for each occupied orbital: 117

$$b_{i}(\tilde{\mathbf{C}}') = 1 - \sum_{\mu \in i} \sum_{\lambda} C'_{\mu i} S_{\mu \lambda} C_{\lambda i}$$
(13)

where i labels the given occupied MO and C is the original MO coefficient matrix. The left-hand sum is limited to those AOs currently contained within the domain of MO i, such that C'_{ui} is an element of the PAO MO coefficient matrix defined in the domain associated with the current iteration. If the chosen subset of atoms and their AOs do not yield a value of b_i below an assigned cutoff, δ_{PAO} , the additional atoms are added in a ranked order (commonly based on atomic Mulliken populations/charges) until the value of b_i converges. Once the domains are assigned, occupied pairs ij are then assigned pair domains based on the union of the domains of the two occupied orbitals, and the number of such pairs included in a given computation is often subject to distance- or energy-based criteria. A key aspect of the PAO approach is that each occupied orbital (or orbital pair) uses a virtual/correlation domain that is taken from a common set of PAOs.

The PAO space contains as many linear dependencies as occupied orbitals, and these are removed by diagonalizing the projected overlap matrix:

$$\tilde{\mathbf{S}}_{ij} = \tilde{\mathbf{C}}_{ij}^{\prime \dagger} \mathbf{S} \tilde{\mathbf{C}}_{ij}^{\prime} \tag{14}$$

where $\tilde{\mathbf{C}}'_{ij}$ contains only the columns for atomic orbitals belonging to the domain of pair ij. PAOs that correspond to eigenvalues of $\tilde{\mathbf{S}}_{ij}$ below a cutoff parameter are removed, and the remaining orbitals are normalized to yield the non-redundant PAO basis for a given pair $\tilde{\mathbf{C}}_{ij}$.

Two matrices are required to transform the MO-basis quantities into the PAO basis. The first, which rotates from the MO basis to the redundant PAO basis for a given pair, is computed as

$$\mathbf{Q}_{ij}^{\mathrm{PAO}} = \mathbf{C}_{ij}^{\dagger} \mathbf{S} \tilde{\mathbf{C}}_{ij}^{\prime} \tag{15}$$

To facilitate the use of the usual orbital energy denominator terms during the update of the amplitude equations at every iteration of the ground-state CC calculation, a semicanonical virtual basis for pair ij, $L_{ij}^{\mathrm{PAO}} = \chi_{ij} \tilde{C}_{ij}$, is found by diagonalizing the Fock matrix in the space of nonredundant PAOs \tilde{F} :

$$\tilde{F}\chi_{ij} = \epsilon_{ij}\chi_{ij} \tag{16}$$

where ϵ_{ij} are the semicanonical orbital energies for the virtual space of occupied pair ij.

2.3.2. Pair Natural Orbitals. In the PNO approach, a compact virtual space is reduced based on density-based criteria rather than spatial extent. Just as in the PAO method, the occupied orbitals are first localized, but then the virtual orbitals are obtained though diagonalization of an approximate density defined in the canonical virtual space for each occupied pair *ij*. The most common choice for this density is that obtained from second-order Møller–Plesset perturbation theory (MP2), viz.,

$$\mathbf{D}_{ij} = \frac{2}{1 + \delta_{ij}} (\mathbf{T}_{ij} \tilde{\mathbf{T}}_{ij}^{\dagger} + \mathbf{T}_{ij}^{\dagger} \tilde{\mathbf{T}}_{ij})$$
(17)

where T_{ij} is the matrix of first-order double-excitation amplitudes and $\tilde{T}_{ij} = 2T_{ij} - T_{ij}^{\dagger}$. Diagonalizing D_{ij} yields the transformation matrix from the virtual MO basis to the PNO basis:

$$\mathbf{D}_{ij}\mathbf{Q}_{ij}^{\text{PNO}} = \mathbf{Q}_{ij}\mathbf{n}_{ij} \tag{18}$$

where \mathbf{n}_{ij} is the diagonal matrix of occupation numbers. Truncation of the space is accomplished by removing PNOs corresponding to occupation numbers below a cutoff, δ_{PNO} . Similarly to the PAO approach, the transformation matrix from the PNO basis to a semicanonical PNO basis for each pair is obtained by diagonalizing the virtual—virtual block of the Fock matrix in the space of PNOs:

$$\tilde{\mathbf{F}}\mathbf{L}_{ij}^{\mathrm{PNO}} = \mathbf{L}_{ij}^{\mathrm{PNO}}\boldsymbol{\epsilon}_{ij} \tag{19}$$

A variant of the PNO space developed by Crawford et al., known as perturbed PNOs or PNO++, has been applied to linear and quadratic response properties in the frequency domain. To improve the ability of the pair density to estimate the relative importance of PNOs to field-dependent quantities, the approximate amplitudes T_{ij} in eq 17 are replaced by approximate *perturbed* amplitudes X_B^{ij} :

$$\mathbf{D}_{ij}(B) = \frac{2}{1 + \delta_{ij}} (\mathbf{X}_{B}^{ij} \tilde{\mathbf{X}}_{B}^{ij\dagger} + \mathbf{X}_{B}^{ij\dagger} \tilde{\mathbf{X}}_{B}^{ij})$$
(20)

with approximate MP2-level perturbed amplitudes created using the Hamiltonian H and perturbation B (chosen to be the electric dipole moment in the length representation) operators, similarity-transformed according to eq 2,

$$X_{ab}^{ij} = \frac{\overline{B}_{ab}^{ij}}{\overline{H}_{aa} + \overline{H}_{bb} - \overline{H}_{ii} - \overline{H}_{jj}}$$
(21)

We note here that ref 107 includes a factor of the field frequency in the denominator in eq 21. As this is generally chosen to be the frequency at which the property is measured and given the broadband nature of the target absorbance and ECD spectra, we have chosen to omit this term. Once created, the perturbed pair density may be used to obtain the PNO++ space in an identical manner to the PNO procedure, which is then truncated using a cutoff $\delta_{\text{PNO++}}$.

3. COMPUTATIONAL DETAILS

We propagated the CC wave function for a helical H_2 tetramer (atomic coordinates are provided in the Supporting Information) for 800 au using a time step of 0.02 au in the presence of a time-dependent electric field. In order to engage all excited states, we approximated a Dirac delta pulse as a narrow Gaussian field of the form

$$E(t) = Fe^{-(t-\nu)^2/2\sigma^2}$$
 (22)

with field strength F, pulse center ν , and standard deviation σ . The field was oriented in the y direction, which was along the helical axis of the system. All calculations in this work used a field defined by $F=1\times 10^{-3}$, $\nu=0.05$, and $\sigma=0.01$, all in atomic units. Time-dependent electric and magnetic dipole moments were damped using a function of the form $e^{-t\tau}$, with $\tau=150$ (where τ has units of inverse atomic units of time). The cc-pVDZ basis set augmented with diffuse functions 119,120 was used throughout.

The reference, PAO, and PNO simulations were performed in the MO space following localization of the occupied orbitals using the Pipek—Mezey procedure. The PAO and PNO simulations were carried out by using domain cutoffs corresponding to successively smaller fractions of the MO virtual space. Truncation of the virtual space is done once and for all by following the ground-state CC procedure. The relative sizes of the remaining virtual spaces are measured by the T_2 ratio, defined as the ratio of the number of doubles amplitudes in the truncated and untruncated spaces. Lower T_2 ratios indicate more aggressive truncation of the virtual space, resulting in potential computational savings. T_2 ratios from 0.05 to 0.95 were explored for each localization scheme.

The effect of truncation of the virtual space was computed using a modified version of our canonical-MO CC code as first described by Hampel and Werner¹²¹ and used in our previous work in reduced-scaling CC methods. ^{105,107,108,122} In each CC iteration or time-propagation step, the amplitude residuals given by eqs 1a and 1b are transformed into the PAO or PNO representation using **Q** and into the semicanonical basis using **L** as

$$\tilde{\mathbf{r}}_i = \mathbf{L}_{ii}^{\mathrm{T}} \mathbf{Q}_{ii}^{\mathrm{T}} \mathbf{r}_i \tag{23a}$$

and

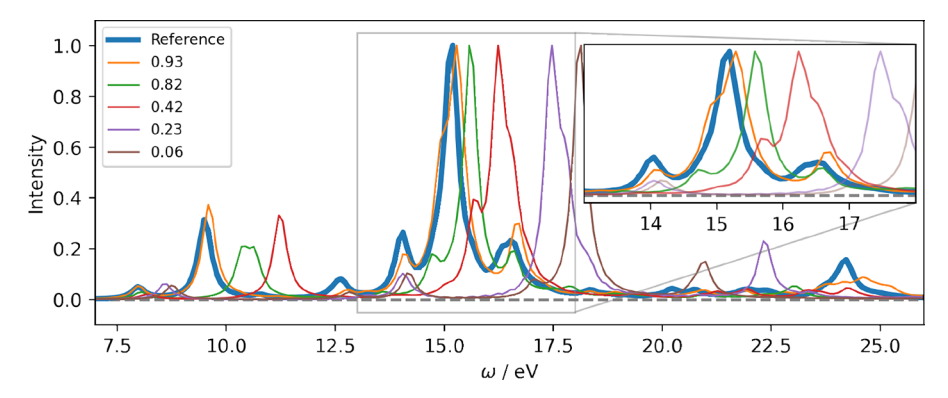


Figure 1. Reference and PAO absorption spectra of $(H_2)_4$ for cutoffs of 1×10^{-4} , 1×10^{-3} , 1×10^{-2} , 5×10^{-2} , and 1×10^{-1} , corresponding to T_2 ratios of 0.93, 0.82, 0.42, 0.23, and 0.06, respectively.

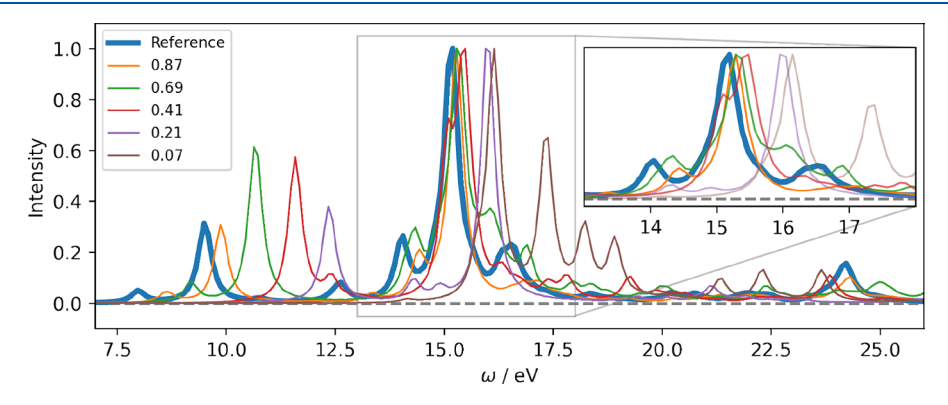


Figure 2. Reference and PNO absorption spectra of $(H_2)_4$ for cutoffs of 1×10^{-10} , 1×10^{-9} , 1×10^{-8} , 1×10^{-7} , and 2×10^{-6} , corresponding to T_2 ratios of 0.87, 0.69, 0.41, 0.21, and 0.07, respectively.

$$\tilde{\mathbf{r}}_{ij} = \mathbf{L}_{ij}^{\mathrm{T}} \mathbf{Q}_{in}^{\mathrm{T}} \mathbf{r}_{ij} \mathbf{Q}_{in} \mathbf{L}_{ij}$$
(23b)

The transformation matrices are computed from either eqs 18 and 19, respectively, for PNOs or eqs 15 and 16, respectively, for PAOs. For the ground-state (time-independent) residuals, the energy denominator is applied in this basis, and then the resulting amplitudes are back-transformed into the MO basis, but for the time-dependent residuals, no such denominators are required, in accord with eq 6. These transformations yield MO-basis amplitudes for which the nonlocal components have been eliminated.

For absorption spectra, the imaginary component of the Fourier transform of the *induced* electric dipole $\tilde{\mu}=(\langle\mu\rangle-\mu_0)$ following an electric-field kick may be directly divided by the Fourier transform of the field strength to yield the spectrum. Electronic CD spectra, however, require the Fourier transform of the time derivative of the field. For a Dirac delta pulse $E_\delta(t)=\kappa\delta(t)$, the Fourier transform of the derivative yields

$$FFT[E_{\delta}] = i\omega\kappa \tag{24}$$

Therefore, for such a field, the CD is proportional to the negative of the *real* part of the Fourier transform of the induced magnetic dipole. In practice, the assumption of a Dirac delta pulse is sufficient provided that a thin Gaussian or Lorentzian pulse is used.

Discrete Fourier transformation was done using a wrapper to the fft submodule of the SciPy Python library. ¹²³ All methods were implemented in the Python-based coupled cluster package, PyCC, ¹²⁴ a NumPy-based ¹²⁵ open-source code developed in the Crawford group for the testing and implementation of novel coupled cluster methods. The code

utilizes the Psi4 electronic structure package ¹²⁶ for integral generation and computing reference wave functions. The RTCC code makes use of the opt_einsum package ¹²⁷ for tensor contractions, and time propagation is performed using an in-house suite of integrators. The integrator used throughout this work was the fourth-order Runge–Kutta method. ¹¹³

4. RESULTS AND DISCUSSION

Here we present results from the first applications of local correlation methods to RTCC. In section 4.1, we examine the convergence of absorption and ECD spectra for a helical hydrogen molecule cluster, compared with canonical (untruncated) RTCC simulations, followed by an analysis of the corresponding cluster amplitude dynamics in section 4.2. In addition, we explore the effect of localization and truncation on the orbital extent in an attempt to explain apparent deficiencies of the PNO space in light of variations in the time-dependent deviations in the amplitudes from the ground state.

4.1. Absorption and ECD Spectra. 4.1.1. Absorption. Absorption spectra are obtained from the Fourier transform of S(t) in eq 10. Figure 1 shows the normalized absorption spectrum obtained from a reference propagation along with five PAO cutoffs, resulting in T_2 ratios ranging from 0.06 to 0.93 (the corresponding δ_{PAO} cutoffs are included in the figure caption).

The largest truncated PAO virtual space, corresponding to a T_2 ratio of 0.93, accurately predicts the excitation energies for each major peak below 17 eV. Convergence to the large reference peak near 15.5 eV occurs from the right, indicating a decrease in excitation energies as the size of the virtual space

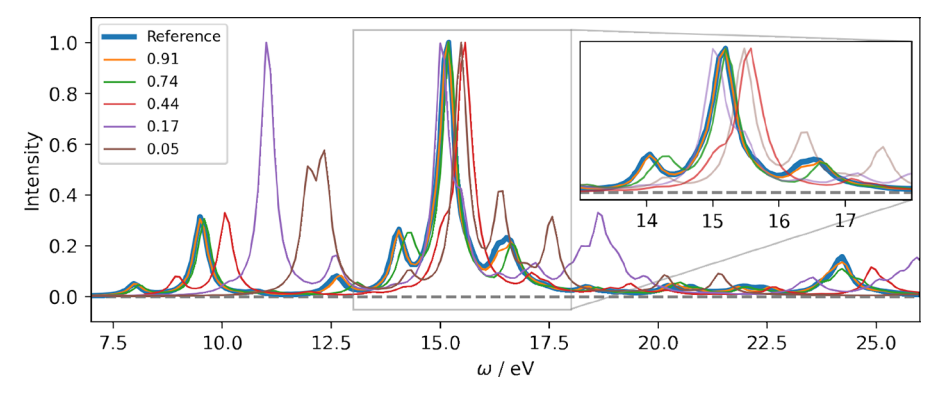


Figure 3. Reference and PNO++ absorption spectra of $(H_2)_4$ for cutoffs of 1×10^{-9} , 1×10^{-8} , 1×10^{-7} , 1×10^{-6} , and 1×10^{-5} , corresponding to T_2 ratios of 0.91, 0.74, 0.44, 0.17, and 0.05, respectively.

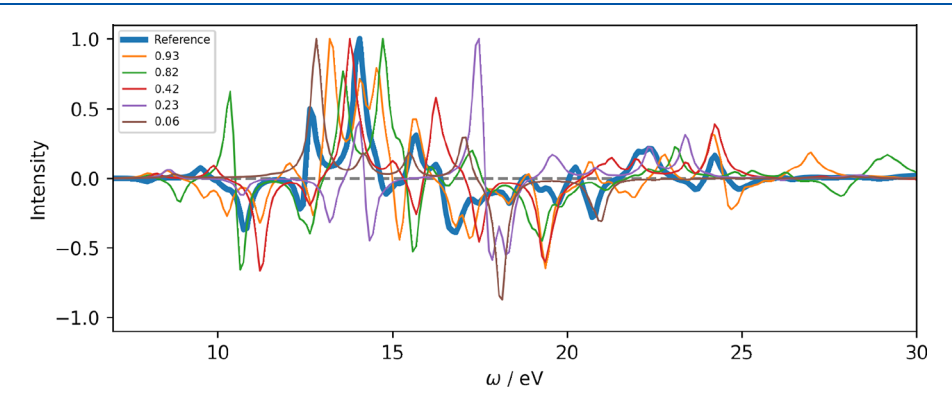


Figure 4. Reference and PAO ECD spectra of $(H_2)_4$ for the cutoffs 1×10^{-4} , 1×10^{-3} , 1×10^{-2} , 5×10^{-2} , and 1×10^{-1} , corresponding to T_2 ratios of 0.93, 0.82, 0.42, 0.23, and 0.06, respectively.

increases. This is the expected trend, as the size of the correlation space for the time-dependent wave function gradually approaches the same quality as the ground-state (unperturbed) wave function and can also be observed for the smaller peak near 10 eV. However, the accuracy of these peaks rapidly declines, e.g. at a ratio of 0.82, where the base peak position is off by approximately 0.5 eV. Performance continues to degrade as the excitation energy increases and the average size of the PAO space decreases. For the final two cutoffs, at T_2 ratios of 0.23 and 0.06, the base peaks are 3 eV or more away from the reference, and no peak is exhibited near 25 eV. These spaces also fail to predict the second-largest peak, occurring just below 10 eV. Thus, while the 0.93 T_2 ratio ($\delta_{PAO} = 10^{-4}$) reproduces the reference spectrum adequately for the lowerenergy peaks, the broadband laser pulse that excites all electronic states puts too great of a burden on the global PAO truncation.

The performance of the PNO approach for the $(H_2)_4$ case is shown in Figure 2. The truncated PNO virtual spaces overestimate the position of the base peak at 15.5 eV, with the smallest space $(T_2=0.07)$ predicting a peak within 1.5 eV of the reference and the two largest spaces $(T_2=0.87)$ and 0.69 predicting this peak to within 0.2 eV of the reference. Even a PNO space with a T_2 ratio of just 0.41 predicts the base-peak position with more accuracy than a PAO space where the T_2 ratio has doubled. However, convergence of the shoulder peaks on either side of the base peak, indicated by the inset of Figure 2, is less predictable. Even the largest spaces considered do not correctly reproduce the excitation energy for these peaks, with no clear advantage to having a T_2 ratio of 0.87 compared to a ratio of just 0.69. This trend continues into

the higher-energy range of the spectrum, with the performances of the various cutoffs being nearly indistinguishable.

Overall, while the PNO basis exhibits improvements for several peaks over the PAO basis, neither scheme produces adequate results upon aggressive truncation of the virtual space. This result is not entirely surprising; in studies of local correlation applied to response theory by Crawford et al., 23,105–108 traditional reduced-scaling approaches proved inaccurate for the closely related electric-dipole polarizability. The perturbation-aware PNO++ space is a promising alternative for such calculations, with results for the absorption spectrum shown in Figure 3.

While aggressive truncation beyond a T_2 ratio of 0.5 is still not feasible, larger PNO++ spaces far outperform their PAO or PNO counterparts. For example, at a T_2 ratio of 0.74, PNO++ provides an improvement over even the largest PAO and PNO spaces tested. Notably, the troublesome peak position near 12.5 eV has improved and nearly overlaps the reference spectrum at a ratio of 0.91. This result corroborates those from frequency-domain studies, suggesting the interchangeability of reduced-scaling methods from frequency- to time-domain CC theory.

4.1.2. ECD. In terms of response theory, absorption is related to the *imaginary* part of the electric dipole—electric dipole linear response tensor (α in eq 9a), while the scalar polarizability and refractive index are related to the *real* part. Indeed, all linear absorptive properties such as absorption and CD are related to the imaginary component of a linear response tensor, while dispersive properties such as refractive index and circular birefringence (also known as optical rotation) are related to the real component. 1,4

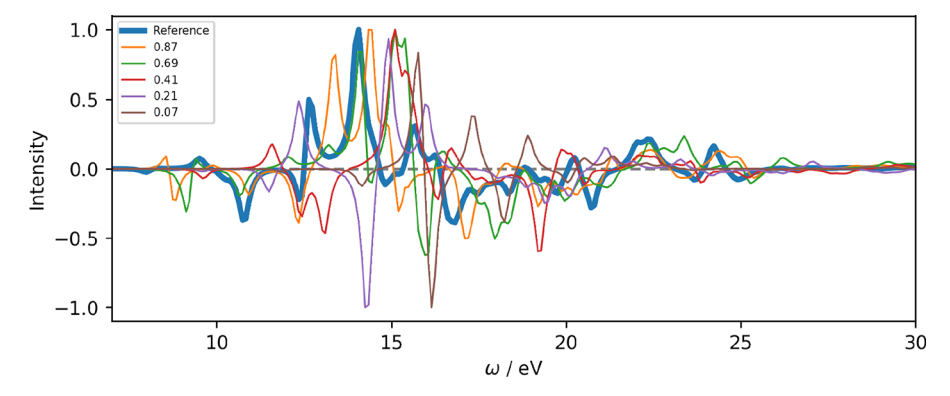


Figure 5. Reference and PNO ECD spectra of $(H_2)_4$ for the cutoffs 1×10^{-10} , 1×10^{-9} , 1×10^{-8} , 1×10^{-7} , and 2×10^{-6} , corresponding to T_2 ratios of 0.87, 0.69, 0.41, 0.21, and 0.07, respectively.

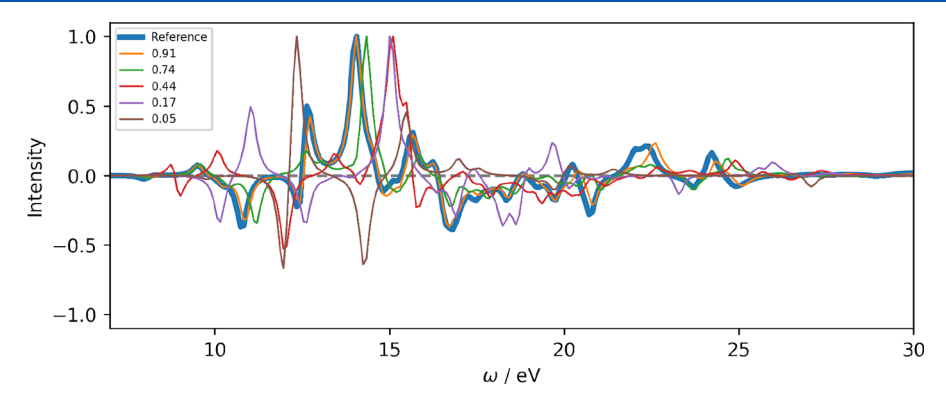


Figure 6. Reference and PNO++ ECD spectra of $(H_2)_4$ for the cutoffs 1×10^{-9} , 1×10^{-8} , 1×10^{-7} , 1×10^{-6} , and 1×10^{-5} , corresponding to T_2 ratios of 0.91, 0.74, 0.44, 0.17, and 0.05, respectively.

The ECD spectrum is obtained from the Fourier transform of $\eta(t)$ in eq 11. Being a bisignate, mixed-response property, ECD is a considerable computational challenge, similar to its dispersive counterpart circular birefringence. Figure 4 shows the results for an ECD spectrum in the same PAO orbital spaces used for the absorption spectrum in the previous section.

The dynamic response of the magnetic dipole to the electric field in this frequency range is considerably more complicated than that of the electric dipole. With even the largest spaces tested, virtually all distinguishing characteristics of the reference spectrum are unidentifiable, and the performance of the PAO basis near the base peak varies wildly with truncation. Curiously, the two largest spaces predict significant peaks above 25 eV that are not present in the reference or the smaller PAO spaces. This indicates a strong sensitivity of the response of the wave function to the completeness threshold used for determining the occupied domains.

Unlike the absorption spectrum, the ECD spectrum does not improve significantly upon switching to the PNO basis, as shown in Figure 5. At a T_2 ratio of 0.87, the overall *shape* of the spectrum in the 10 to 20 eV range more closely resembles that of the reference; however, the excitation energies are in some cases even less accurate than those of smaller PNO spaces, and the trend of lowering excited-state energies with increased virtual space seen in section 4.1.1 is no longer discernible.

Finally, Figure 6 reports ECD spectra obtained upon truncation of the PNO++ spaces used in the previous section. As expected based on frequency-domain results, ^{23,105-108} ECD proves to be a greater challenge for the PNO++ method than absorption. However, there are still marked improvements

compared to PAO and PNO. At a T_2 ratio of 0.74, most distinguishing features of the spectrum below 20 eV are present. The only notable exception to this is the Cotton feature located near 12.5 eV, which is recovered when the T_2 ratio is 0.91. As with absorption, while one cannot truncate as aggressively as when performing energy calculations, these results show a clear benefit to including the response to the perturbation when building new virtual orbital spaces for reduced-scaling techniques.

4.2. Amplitude Dynamics. As evidenced by the preceding data, the truncated PAO and PNO virtual spaces do not efficiently model the wave function in the presence of a perturbing EMF. As noted in section 4.1.2, these shortcomings are well-documented in the case of response theory. Including the effects of the perturbation through the PNO++ approach improves results, although possible truncations still fall short of those used for energy calculations. However, a real-time formalism offers the opportunity to analyze the wave function dynamics in great detail, perhaps shedding light on *where* and *how* the locally correlated wave functions are deficient. The following section will scrutinize the t_{μ} and λ_{μ} amplitudes of eqs 3b and 4b, respectively, in order to determine the important fluctuations in the wave function and whether these spaces sufficiently capture these changes.

Response to external perturbations by the CC amplitudes gives rise to dynamic energetics and properties. In the past, distributions of perturbed amplitudes (relative to their ground-state counterparts) have been used to justify the difficulty in computing response functions with local correlation methods in the frequency domain. However, initial findings show that in RTCC, the relative distribution of amplitudes by

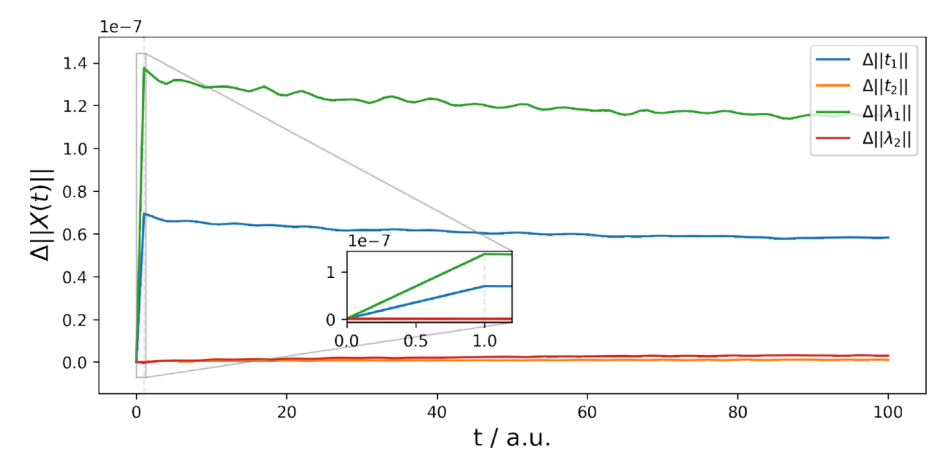


Figure 7. Time-dependent changes in the norms of the amplitude tensors relative to the ground-state amplitudes. Field and step parameters remain unchanged, and the amplitude norms are taken at every 1 au.

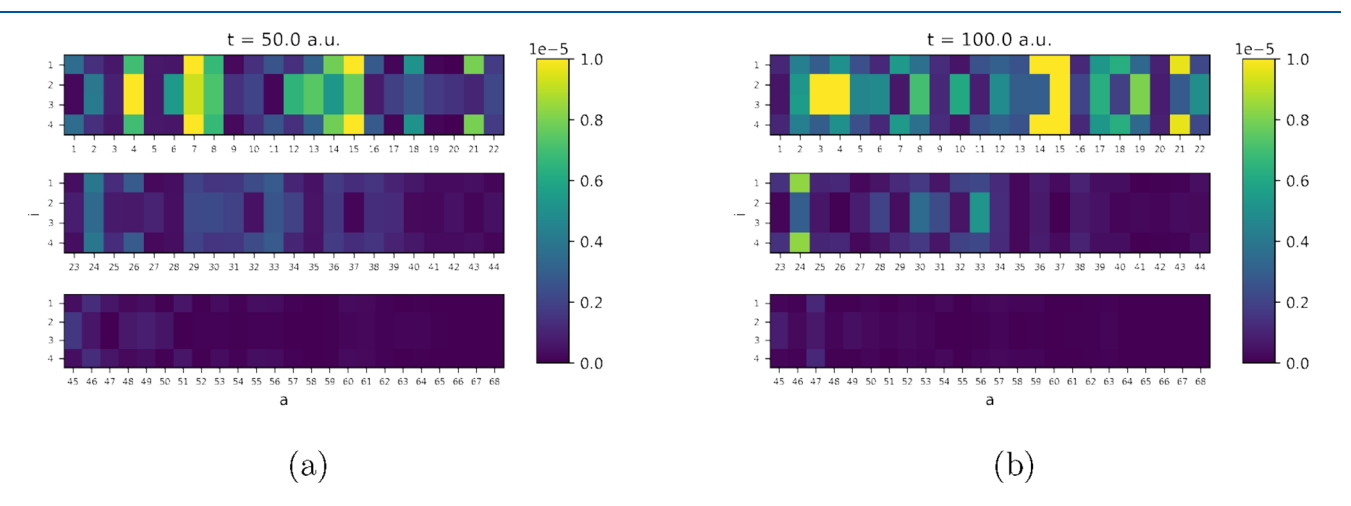


Figure 8. MO-basis λ_1 amplitude deviations from t = 0 after (a) 50 au and (b) 100 au of time propagation. Each row contains the same four localized occupied orbital indices and a subset of virtual indices as indicated by the x-axis labels, given in order of increasing orbital energy.

magnitude is not significantly impacted.²³ Despite this, typical means of exploiting amplitude sparsity have been shown to be inefficient in the preceding sections. First, to understand the response of the amplitudes to the external perturbation, we plot the change in the norm of the singles- and doubles-amplitude tensors relative to the unperturbed ground-state amplitudes as a function of time in Figure 7. Results for the reduced-scaling spaces are identical to those for the MO space, as the unitary transformations resulting from untruncated localized virtual spaces in eqs 23 preserve the tensor norm.

Figure 7 shows that the largest component of the response by the wave function is predominantly within the single amplitudes t_1 and λ_1 . This is consistent with the notion that singles are paramount for the computation of response properties. However, the density in eq 17 does not include any contributions by singles since it is built from MP2-level (perturbed) amplitudes, where singles do not contribute until at least the second order in the wave function and fourth order in the energy. This suggests that even in schemes that seek to include the EMF perturbation in the construction of the reduced virtual space, such as PNO++, response of the singles should be considered, and this may provide significant improvements.

In addition to the matrix norm, we can also inspect the individual amplitudes to track their evolution in time. The heat

maps in Figure 8 show the difference in λ_1 amplitudes in the MO basis relative to the ground state for t = 50 au and t = 100au to investigate deviations in the amplitudes far from the initial electric field pulse. The amplitudes are ordered by the energies of the associated MOs. Those amplitudes that experience significant oscillations vary throughout the simulation, although there are several discernible trends. The same trends were observed in both the λ_1 and t_1 amplitudes only the λ_1 amplitudes are discussed here for brevity. First, most large amplitude deviations are associated with all occupied orbitals simultaneously. This is due to the relatively small size of the system, with only four occupied orbitals, all of which are likely important in the description of the groundand excited-state wave functions. Second, at any given time during propagation, a large number of amplitudes do not significantly deviate from their ground-state values. This supports the notion that the relative sparsity of the wave function is maintained within the amplitudes throughout the simulation but that this sparsity is distributed differently throughout the amplitude tensors as the wave function is propagated.

A third trend is that amplitudes that respond strongly tend to be associated with low-energy virtual orbitals. Chemical intuition would suggest that energetically low-lying molecular orbitals will be the most involved in electronic excitations,

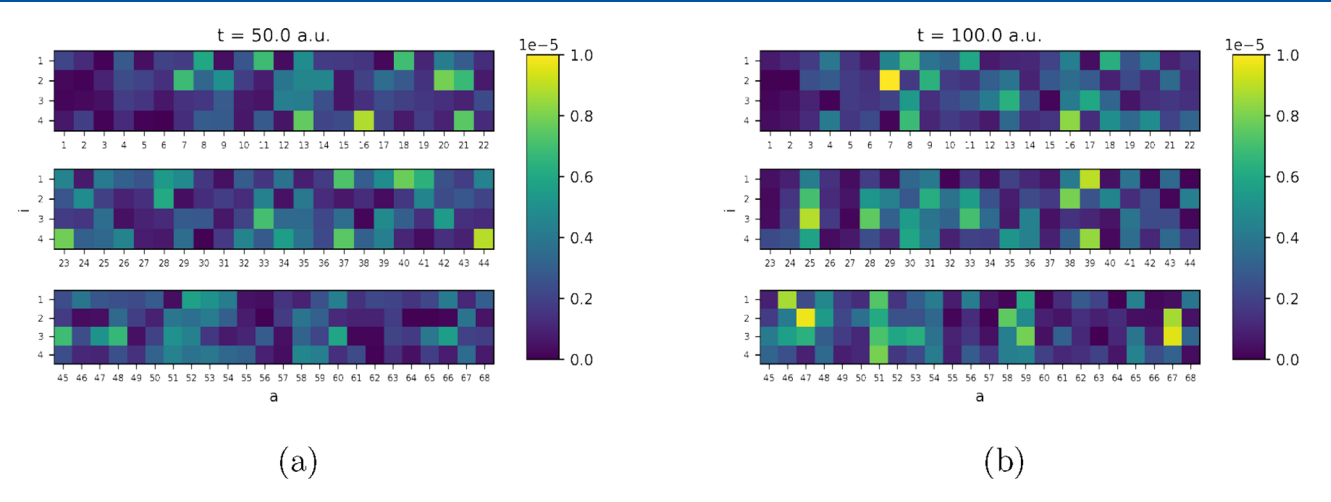


Figure 9. PNO-basis λ_1 amplitude deviations from t = 0 after (a) 50 au and (b) 100 au of time propagation. Each row contains the same four occupied orbital indices and a subset of virtual indices as indicated by the x-axis labels, given in order of increasing orbital energy.

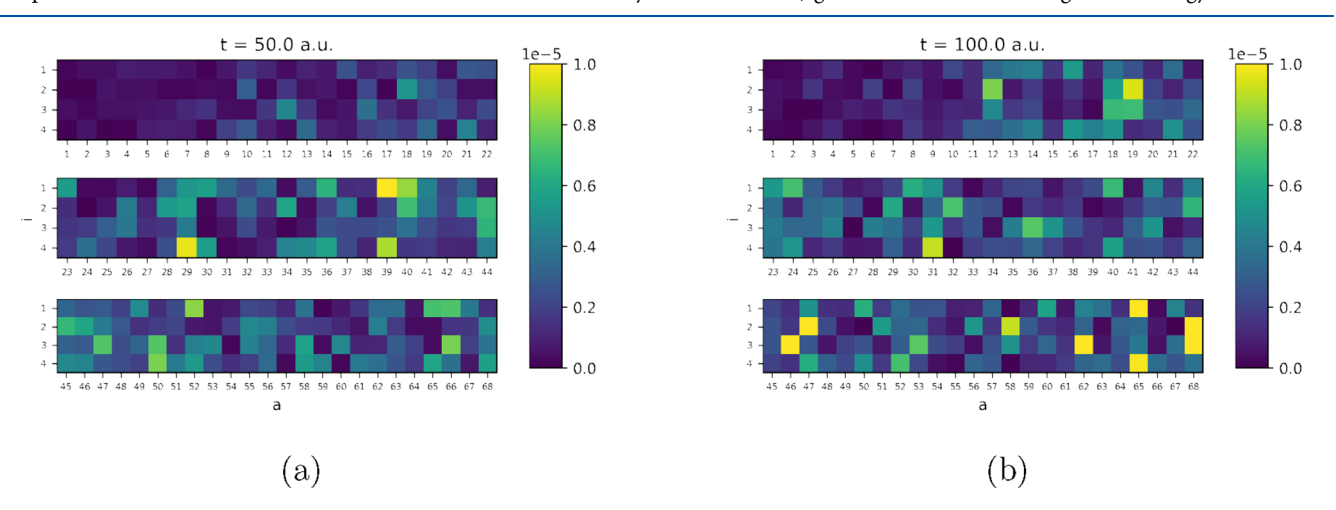


Figure 10. PNO++-basis λ_1 amplitude deviations from t = 0 after (a) 50 au and (b) 100 au of time propagation. Each row contains the same four occupied orbital indices and a subset of virtual indices as indicated by the x-axis labels.

particularly for valence states. However, while amplitude responses are indeed larger for lower-energy virtual orbitals, the smaller amplitude deviations in Figure 8 extend far into the virtual space. This explains the difficulty of simply truncating with respect to orbital energy: the high-energy MOs are still important to the time evolution of the wave function in the presence of an EMF.

Figure 9 shows the λ_1 amplitudes for the same simulation, rotated into the untruncated PNO basis using Q_{ii} as defined in eq 18. (It should be noted that due to redundancy in the AO-based virtual spaces for each pair, PAO-basis amplitudes cannot be compared directly in this manner.) It can be immediately seen that the amplitude deviations are significantly less sparse in the PNO basis after the application of the EMF. Many more amplitudes exhibit perceivable differences, and strong deviations (magnitudes approaching 1×10^{-5}) are no longer present. This is a clear demonstration of the issue with truncating orbital spaces based on the present criterion—rather than exploiting sparsity, the amplitude tensors have become less sparse.

Finally, amplitude plots in the PNO++ basis are shown in Figure 10. We find that some sparsity has been retained; however, these amplitudes are still not as sparse or as ordered as those in Figure 8. The improvements of the PNO++ basis

relative to the PNO basis are likely due to this more efficient representation of the wave function amplitudes.

The virtual orbital spatial extent has been used previously 106,107 to estimate the ability of locally correlated spaces to describe the diffuse regions of electron density that are important for response properties. Figure 11 shows the virtual MO energy ϵ_a and the PNO occupation number n_a plotted against the orbital extent $\langle r^2 \rangle$ in atomic units. In the PNO basis, a unique virtual space is prepared for every occupied pair, resulting in 10 unique spaces for the four occupied spatial orbitals i. However, for transforming a single orbital index, we only require the diagonal rotation matrices (i.e., Q_{ii}). There are four such spaces; however, by symmetry, only two are unique, and both are included in Figure 11.

Truncation of the PNO space begins from the bottom of Figure 11, e.g., at an occupation number cutoff of 1×10^{-9} (indicated by a horizontal line), all orbitals below this line are neglected in the PNO space. This results in the PNO space with a T_2 ratio of 0.69. From these data, it is clear that even modest truncation of the virtual space neglects the diffuse regions of the wave function, which are important for excited-state properties in systems with significantly delocalized characteristics, such as systems containing Rydberg-type excitations.

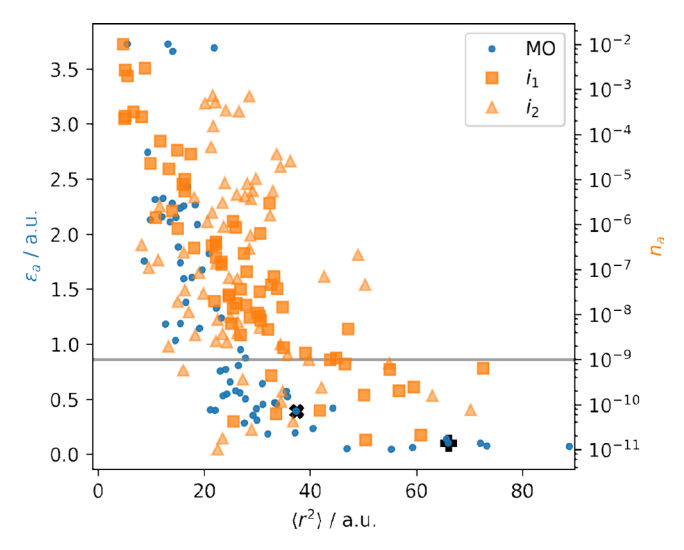


Figure 11. Virtual MO energy ϵ_a (left-hand axis) and PNO occupation number n_a (right-hand axis, plotted on a log scale) for unique PNO spaces i_1 and i_2 versus orbital extent. Virtual MOs 7 and 15 are denoted by a solid + and \times , respectively. The horizontal line denotes a PNO cutoff of 1×10^{-9} .

The same analysis can be performed for the PNO++ virtual spaces in Figure 12. The horizontal line indicates a cutoff of 1

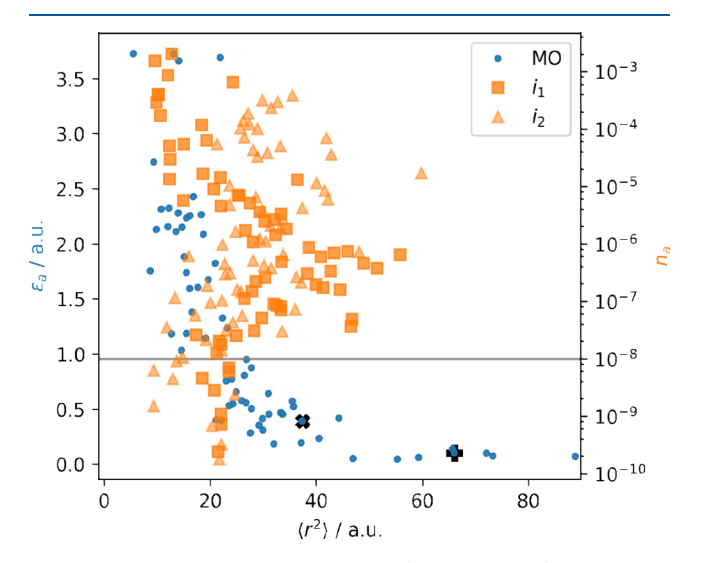


Figure 12. Virtual MO energy ϵ_a (left-hand axis) and PNO occupation number n_a (right-hand axis, plotted on a log scale) for unique PNO++ spaces i_1 and i_2 versus orbital extent. Virtual MOs 7 and 15 are denoted by a solid + and \times , respectively. The horizontal line denotes a PNO++ cutoff of 1×10^{-8} .

 \times 10⁻⁸, corresponding to a T_2 ratio of 0.74. Below this threshold, at which point the quality of the absorption and ECD spectra in Figures 3 and 6 begins to deteriorate rapidly, more diffuse orbitals begin to be neglected. This strongly alludes to the nature of the excited states and suggests that spatial extent may be an important criterion to consider in future work.

Spatial extent alone may not be a suitable criterion for truncation—this would have a negative impact on the accuracy of the correlation energy, which is inherently local in nature for molecules with isolated ground states. Additionally, spatially compact orbitals may contribute significantly to the response

of the wave function. Figures 11 and 12 highlight virtual MOs 7 (+) and 15 (×), which involve the strongest deviations in Figures 8a and 8b, respectively. These deviations represent a strong response of the wave function to the perturbing field, implying that they are of particular importance when computing dynamic properties. Examination of the spatial extents of these orbitals, in particular, may shed light on the nature of the spatial distribution of orbitals necessary to describe the wave function response. Virtual MO 7 appears at 66 au, while MO 15 is nearly half that at 37 au. That these orbitals are of such varying extents demonstrates that both diffuse and compact orbitals play a role in the wave function dynamics.

5. CONCLUSIONS

We have presented the first application of local correlation concepts to RTCC simulations. The popular PAO and PNO virtual space localization schemes have been applied to the calculation of dynamic electric and magnetic dipole moments in the presence of an explicit electric field, providing absorption and ECD spectra, respectively. For a helical H₂ tetramer test case, truncation of the localized virtual space to successively larger fractions of the canonical virtual space resulted in convergence to the canonical result; however, this convergence is slow, and errors in excitation energies and intensity are present even in some of the largest spaces tested, especially for ECD. The recently developed PNO++ scheme has been shown to improve convergence significantly. This corroborates the results of recent studies applying locally correlated methods to the prediction of dynamic properties in the frequency domain using response theory. However, more work is needed to achieve the desired balance of accuracy and computational cost.

Examining the amplitude dynamics during the propagation, it has been shown that the t_1 and λ_1 amplitudes respond most strongly to the field; a large increase in the norm of these matrices is observed upon application of the field, followed by a steady oscillation. The t_2 and λ_2 tensors, in comparison, remain relatively static throughout. These oscillations are largely, but not completely, localized to a selection of only a few orbitals, as evidenced by the consideration of time-dependent deviations in the λ_1 amplitudes from the ground state. In the localized virtual spaces tested, these oscillations are delocalized throughout the t_1 and λ_1 matrices to different degrees, with the PNO++ virtual space retaining more sparsity than the PNO space.

Orbital extent alone cannot explain the shortcomings of the locally correlated methods explored here, although its effect is significant. These results provide an insight into the importance of singly substituted determinants in the timedependent wave function in the presence of an electric field as well as a potential metric to gauge the performance of new localization schemes for frequency- or time-domain calculations of dynamic response properties. In order to attain a balanced description of wave function components important for both energy and property calculations, the combination of appropriately determined spaces such as the combined PNO+ + approach has been fruitful. 107,108 Still neglected in this approach are the singles amplitudes, which are absent in the MP2 wave functions used to approximate the occupied pair domains. Schemes to include these effects, such as approximate CC2-level t_1 guess amplitudes, may further improve the space and allow greater flexibility for truncation. In addition, rather

than the broadband Dirac delta pulse used for the external electric field, more complex experimental setups may prove to be amenable to such truncation. Longer time-domain pulses that target specific frequency regions for X-ray core excitations, for example, could permit a more aggressive truncation of the wave function. The prospect of using these methodologies within the current framework is promising, and work is underway to explore their efficiency and efficacy.

ASSOCIATED CONTENT

Solution Supporting Information

The Supporting Information is available free of charge at https://pubs.acs.org/doi/10.1021/acs.jpca.3c05151.

Coordinates of the helical hydrogen tetramer, $(H_2)_4$ (XYZ)

AUTHOR INFORMATION

Corresponding Author

- T. Daniel Crawford Department of Chemistry, Virginia Tech, Blacksburg, Virginia 24061, United States;
 occid.org/0000-0002-7961-7016; Email: crawdad@
 - vt.edu

Authors

Benjamin G. Peyton – Department of Chemistry, Virginia Tech, Blacksburg, Virginia 24061, United States Zhe Wang – Department of Chemistry, Virginia Tech, Blacksburg, Virginia 24061, United States

Complete contact information is available at: https://pubs.acs.org/10.1021/acs.jpca.3c05151

Notes

The authors declare no competing financial interest.

ACKNOWLEDGMENTS

This work was supported by the U.S. National Science Foundation via Grant CHE-2136142. The authors gratefully acknowledge Advanced Research Computing at Virginia Tech for providing computational resources and technical support that contributed to the results reported within the paper.

REFERENCES

- (1) Barron, L. D. Molecular Light Scattering and Optical Activity, 2nd ed.; Cambridge University Press, 2004.
- (2) Goddard, W. A. Theoretical chemistry comes alive: Full partner with experiment. *Science* **1985**, *227*, 917–923.
- (3) Crawford, T. D. Ab initio calculation of molecular chiroptical properties. *Theor. Chem. Acc.* **2006**, *115*, 227–245.
- (4) Norman, P. A perspective on nonresonant and resonant electronic response theory for time-dependent molecular properties. *Phys. Chem. Chem. Phys.* **2011**, *13*, 20519.
- (5) Helgaker, T.; Coriani, S.; Jørgensen, P.; Kristensen, K.; Olsen, J.; Ruud, K. Recent advances in wave function-based methods of molecular-property calculations. *Chem. Rev.* **2012**, *112*, 543–631.
- (6) McLachlan, A. D. A variational solution of the time-dependent Schödinger equation. *Mol. Phys.* **1964**, *8*, 39–44.
- (7) Jørgensen, P. Molecular and Atomic Applications of Time-Dependent Hartree-Fock Theory. *Annu. Rev. Phys. Chem.* **1975**, 26, 359–380.
- (8) Oddershede, J. Polarization Propagator Calculations. *Adv. Quantum Chem.* **1978**, *11*, 275–352.
- (9) Jørgensen, P.; Simons, J. Second Quantization-Based Methods in Quantum Chemistry; Academic Press: New York, 1981.

- (10) Linderberg, J.; Öhrn, Y. Propagators in Quantum Chemistry, 2nd ed.; Wiley: Hoboken, NJ, 2004.
- (11) Schirmer, J. Beyond the random-phase approximation: A new approximation scheme for the polarization propagator. *Phys. Rev. A* **1982**, 26, 2395–2416.
- (12) Wormit, M.; Rehn, D. R.; Harbach, P. H.; Wenzel, J.; Krauter, C. M.; Epifanovsky, E.; Dreuw, A. Investigating excited electronic states using the algebraic diagrammatic construction (ADC) approach of the polarisation propagator. *Mol. Phys.* **2014**, *112*, 774–784.
- (13) Dreuw, A.; Wormit, M. The algebraic diagrammatic construction scheme for the polarization propagator for the calculation of excited states. *Wiley Interdiscip. Rev.: Comput. Mol. Sci.* **2015**, *5*, 82–95.
- (14) Olsen, J.; Jørgensen, P. Linear and nonlinear response functions for an exact state and for an MCSCF state. *J. Chem. Phys.* **1985**, *82*, 3235–3264.
- (15) Casida, M. E. Time-Dependent Density Functional Response Theory for Molecules. In *Recent Advances in Density Functional Methods*; Chong, D. P., Ed.; World Scientific: Singapore, 1995; Vol. 1, Chapter 5, pp 155–192.
- (16) Rice, J. E.; Handy, N. C. The calculation of frequency-dependent polarizabilities and pseudo-energy derivatives. *J. Chem. Phys.* **1991**, *94*, 4959–4971.
- (17) Aiga, F.; Itoh, R. Calculation of frequency-dependent polarizability and hyperpolarizabilities by the second-order Møller-Plesset perturbation theory. *Chem. Phys. Lett.* **1996**, *251*, 372–380.
- (18) Norman, P. A perspective on nonresonant and resonant electronic response theory for time-dependent molecular properties. *Phys. Chem. Phys.* **2011**, *13*, 20519–20535.
- (19) Norman, P.; Ruud, K.; Saue, T. Principles and Practices of Molecular Properties: Theory, Modeling, and Simulations; John Wiley and Sons: Hoboken, NJ, 2018.
- (20) Koch, H.; Jørgensen, P. Coupled cluster response functions. *J. Chem. Phys.* **1990**, 93, 3333–3344.
- (21) Pedersen, T. B.; Koch, H. Coupled cluster response functions revisited. *J. Chem. Phys.* **1997**, *106*, 8059–8072.
- (22) Crawford, T. D. Frontiers of Coupled Cluster Chiroptical Response Theory. In *Frontiers of Quantum Chemistry*; Wójcik, M. J., Nakatsuji, H., Kirtman, B., Ozaki, Y., Eds.; Springer: Singapore, 2018; pp 49–68.
- (23) Crawford, T. D.; Kumar, A.; Bazanté, A. P.; Di Remigio, R. Reduced-scaling coupled cluster response theory: Challenges and opportunities. *Wiley Interdiscip. Rev.: Comput. Mol. Sci.* **2019**, *9*, e1406.
- (24) Langhoff, P. W.; Epstein, S. T.; Karplus, M. Aspects of time-dependent perturbation theory. *Rev. Mod. Phys.* 1972, 44, 602–644.
- (25) Goings, J. J.; Lestrange, P. J.; Li, X. Real-time time-dependent electronic structure theory. *Wiley Interdiscip. Rev.: Comput. Mol. Sci.* **2018**, *8*, e1341.
- (26) Li, X.; Govind, N.; Isborn, C.; DePrince, A. E., III; Lopata, K. Real-Time Time-Dependent Electronic Structure Theory. *Chem. Rev.* **2020**, *120*, *9951*–*9993*.
- (27) Maiuri, M.; Garavelli, M.; Cerullo, G. Ultrafast Spectroscopy: State of the Art and Open Challenges. *J. Am. Chem. Soc.* **2020**, *142*, 3–15.
- (28) Lewenstein, M.; Balcou, P.; Ivanov, M. Y.; L'Huillier, A.; Corkum, P. B. Theory of high-harmonic generation by low-frequency laser fields. *Phys. Rev. A* **1994**, *49*, 2117–2132.
- (29) Gorlach, A.; Neufeld, O.; Rivera, N.; Cohen, O.; Kaminer, I. The quantum-optical nature of high harmonic generation. *Nat. Commun.* **2020**, *11*, 4598.
- (30) Yabana, K.; Bertsch, G. Time-dependent local-density approximation in real time. *Phys. Rev. B: Condens. Matter Mater. Phys.* **1996**, *54*, 4484–4487.
- (31) Yabana, K.; Bertsch, G. F. Optical response of small carbon clusters. Z. Phys. D: Atoms Mol. Clust. 1997, 42, 219–225.
- (32) Yabana, K.; Bertsch, G. F. Time-dependent local-density approximation in real time: Application to conjugated molecules. *Int. J. Quantum Chem.* **1999**, *75*, 55–66.

- (33) Bertsch, G. F.; Iwata, J. I.; Rubio, A.; Yabana, K. Real-space, real-time method for the dielectric function. *Phys. Rev. B: Condens. Matter Mater. Phys.* **2000**, *62*, 7998–8002.
- (34) Lopata, K.; Govind, N. Modeling fast electron dynamics with real-time time-dependent density functional theory: Application to small molecules and chromophores. *J. Chem. Theory Comput.* **2011**, *7*, 1344–1355.
- (35) Castro, A.; Rubio, A.; Gross, E. K. Enhancing and controlling single-atom high-harmonic generation spectra: a time-dependent density-functional scheme. *Eur. Phys. J. B* **2015**, *88*, 191.
- (36) Tussupbayev, S.; Govind, N.; Lopata, K.; Cramer, C. J. Comparison of real-time and linear-response time-dependent density functional theories for molecular chromophores ranging from sparse to high densities of states. *J. Chem. Theory Comput.* **2015**, *11*, 1102–1109.
- (37) Goings, J. J.; Li, X. An atomic orbital based real-time time-dependent density functional theory for computing electronic circular dichroism band spectra. *J. Chem. Phys.* **2016**, *144*, 234102.
- (38) Bruner, A.; Lamaster, D.; Lopata, K. Accelerated Broadband Spectra Using Transition Dipole Decomposition and Padé Approximants. *J. Chem. Theory Comput.* **2016**, *12*, 3741–3750.
- (39) Sun, S.; Beck, R. A.; Williams-Young, D.; Li, X. Simulating Magnetic Circular Dichroism Spectra with Real-Time Time-Dependent Density Functional Theory in Gauge including Atomic Orbitals. *J. Chem. Theory Comput.* **2019**, *15*, 6824–6831.
- (40) Ding, F.; Van Kuiken, B. E.; Eichinger, B. E.; Li, X. An efficient method for calculating dynamical hyperpolarizabilities using real-time time-dependent density functional theory. *J. Chem. Phys.* **2013**, *138*, No. 064104.
- (41) Repisky, M.; Konecny, L.; Kadek, M.; Komorovsky, S.; Malkin, O. L.; Malkin, V. G.; Ruud, K. Excitation Energies from Real-Time Propagation of the Four-Component Dirac-Kohn-Sham Equation. *J. Chem. Theory Comput.* **2015**, *11*, 980–991.
- (42) Kadek, M.; Konecny, L.; Gao, B.; Repisky, M.; Ruud, K. X-ray absorption resonances near L2,3-edges from real-time propagation of the Dirac-Kohn-Sham density matrix. *Phys. Chem. Chem. Phys.* **2015**, 17, 22566–22570.
- (43) Peach, M. J. G.; Benfield, P.; Helgaker, T.; Tozer, D. J. Excitation energies in density functional theory: An evaluation and a diagnostic test. *J. Chem. Phys.* **2008**, *128*, No. 044118.
- (44) Fuks, J. İ.; Elliott, P.; Rubio, A.; Maitra, N. T. Dynamics of charge-transfer processes with time-dependent density functional theory. *J. Phys. Chem. Lett.* **2013**, *4*, 735–739.
- (45) Fuks, J. I.; Luo, K.; Sandoval, E. D.; Maitra, N. T. Timeresolved spectroscopy in time-dependent density functional theory: An exact condition. *Phys. Rev. Lett.* **2015**, *114*, 183002.
- (46) Hoodbhoy, P.; Negele, J. W. Time-dependent coupled-cluster approximation to nuclear dynamics. I. Application to a solvable model. *Phys. Rev. C* **1978**, *18*, 2380–2394.
- (47) Hoodbhoy, P.; Negele, J. W. Time-dependent coupled-cluster approximation to nuclear dynamics. II. General formulation. *Phys. Rev.* C **1979**, *19*, 1971–1982.
- (48) Schönhammer, K.; Gunnarsson, O. Time-dependent approach to the calculation of spectral functions. *Phys. Rev. B* **1978**, *18*, 6606–6614.
- (49) Arponen, J. S. Variational principles and linked-cluster exp *S* expansions for static and dynamic many-body problems. *Ann. Phys.* **1983**, *151*, 311.
- (50) Huber, C.; Klamroth, T. Explicitly time-dependent coupled cluster singles doubles calculations of laser-driven many-electron dynamics. *J. Chem. Phys.* **2011**, *134*, 054113.
- (51) Kvaal, S. Ab initio quantum dynamics using coupled-cluster. J. Chem. Phys. 2012, 136, 194109.
- (52) Nascimento, D. R.; DePrince, A. E., III. A general time-domain formulation of equation-of-motion coupled-cluster theory for linear spectroscopy. *J. Chem. Phys.* **2019**, *151*, 204107.
- (53) Pedersen, T. B.; Kvaal, S. Symplectic integration and physical interpretation of time-dependent coupled-cluster theory. *J. Chem. Phys.* **2019**, *150*, 144106.

- (54) Park, Y. C.; Perera, A.; Bartlett, R. J. Equation of motion coupled-cluster for core excitation spectra: Two complementary approaches. *J. Chem. Phys.* **2019**, *151*, 164117.
- (55) Pathak, H.; Panyala, A.; Peng, B.; Bauman, N. P.; Mutlu, E.; Rehr, J. J.; Vila, F. D.; Kowalski, K. Real-Time Equation-of-Motion Coupled-Cluster Cumulant Green's Function Method: Heterogeneous Parallel Implementation Based on the Tensor Algebra for Many-Body Methods Infrastructure. *J. Chem. Theory Comput.* **2023**, 19, 2248–2257. PMID: 37096369
- (56) Kristiansen, H. E.; Schøyen, Ø. S.; Kvaal, S.; Pedersen, T. B. Numerical stability of time-dependent coupled-cluster methods for many-electron dynamics in intense laser pulses. *J. Chem. Phys.* **2020**, 152, No. 071102.
- (57) Pedersen, T. B.; Kristiansen, H. E.; Bodenstein, T.; Kvaal, S.; Schøyen, Ø. S. Interpretation of Coupled-Cluster Many-Electron Dynamics in Terms of Stationary States. *J. Chem. Theory Comput.* **2021**, *17*, 388–404.
- (58) Nascimento, D. R.; DePrince, A. E. Linear Absorption Spectra from Explicitly Time-Dependent Equation-of-Motion Coupled-Cluster Theory. *J. Chem. Theory Comput.* **2016**, *12*, 5834–5840.
- (59) Nascimento, D. R.; Deprince, A. E. Simulation of Near-Edge X-ray Absorption Fine Structure with Time-Dependent Equation-of-Motion Coupled-Cluster Theory. *J. Phys. Chem. Lett.* **2017**, *8*, 2951–2957
- (60) Park, Y. C.; Perera, A.; Bartlett, R. J. Equation of motion coupled-cluster study of core excitation spectra II: Beyond the dipole approximation. *J. Chem. Phys.* **2021**, *155*, No. 094103.
- (61) Sato, T.; Pathak, H.; Orimo, Y.; Ishikawa, K. L. Communication: Time-dependent optimized coupled-cluster method for multielectron dynamics. *J. Chem. Phys.* **2018**, *148*, No. 051101.
- (62) Christiansen, O.; Koch, H.; Jørgensen, P. The second-order approximate coupled cluster singles and doubles model CC2. *Chem. Phys. Lett.* **1995**, 243, 409–418.
- (63) Koch, H.; Christiansen, O.; Jørgensen, P.; Sanchez De Merás, A. M.; Helgaker, T. The CC3 model: An iterative coupled cluster approach including connected triples. *J. Chem. Phys.* **1997**, *106*, 1808–1818.
- (64) Wolinski, K.; Hinton, J. F.; Pulay, P. Efficient Implementation of the Gauge-Independent Atomic Orbital Method for NMR Chemical Shift Calculations. *J. Am. Chem. Soc.* **1990**, *112*, 8251–8260.
- (65) Sadlej, A. J. Molecular Electric Polarizabilities. Electric-Field-Variant (EFV) Gaussian Basis Set for Polarizability Calculations. *Chem. Phys. Lett.* **1977**, *47*, 50–54.
- (66) Roos, B. O.; Sadlej, A. J. Polarized basis sets for accurate predictions of molecular electric properties. Electric moments of the LiH molecule. *Chem. Phys.* **1985**, *94*, 43–53.
- (67) Sadlej, A. J. Medium-size polarized basis sets for high-level-correlated calculations of molecular electric properties II. Second-row atoms: Si through Cl. *Theor. Chim. Acta* **1991**, *79*, 123–140.
- (68) Benkova, Z.; Sadlej, A. J.; Oakes, R. E.; Bell, S. E. Reduced-size polarized basis sets for calculations of molecular electric properties. I. the basis set generation. *J. Comput. Chem.* **2005**, *26*, 145–153.
- (69) Baranowska, A.; Sadlej, A. J. Polarized Basis Sets for Accurate Calculations of Static and Dynamic Electric Properties of Molecules. *J. Comput. Chem.* **2009**, *31*, 552–560.
- (70) Baranowska-Łączkowska, A.; Łączkowski, K. Z. The ORP basis set designed for optical rotation calculations. *J. Comput. Chem.* **2013**, 34, 2006–2013.
- (71) Aharon, T.; Caricato, M. Compact Basis Sets for Optical Rotation Calculations. *J. Chem. Theory Comput.* **2020**, *16*, 4408–4415.
- (72) Howard, J. C.; Sowndarya S. V., S.; Ansari, I. M.; Mach, T. J.; Baranowska-Łączkowska, A.; Crawford, T. D. Performance of Property-Optimized Basis Sets for Optical Rotation with Coupled Cluster Theory. *J. Phys. Chem. A* **2018**, *122*, 5962–5969.
- (73) Wang, Z.; Peyton, B. G.; Crawford, T. D. Accelerating Real-Time Coupled Cluster Methods with Single-Precision Arithmetic and Adaptive Numerical Integration. *J. Chem. Theory Comput.* **2022**, *18*, 5479–5491.

- (74) Pulay, P. Localizability of dynamic electron correlation. *Chem. Phys. Lett.* **1983**, *100*, 151–154.
- (75) Stoll, H. On the correlation energy of graphite. *J. Chem. Phys.* **1992**, 97, 8449–8454.
- (76) Saebø, S.; Pulay, P. Local Treatment of Electron Correlation. *Annu. Rev. Phys. Chem.* **1993**, 44, 213–236.
- (77) Hampel, C.; Werner, H.-J. Local treatment of electron correlation in coupled cluster theory. *J. Chem. Phys.* **1996**, *104*, 6286–6297.
- (78) Schütz, M.; Hetzer, G.; Werner, H.-J. Low-order scaling local electron correlation methods. I. Linear scaling local MP2. *J. Chem. Phys.* **1999**, *111*, 5691–5705.
- (79) Schütz, M.; Werner, H.-J. Local perturbative triples correction (T) with linear cost scaling. *Chem. Phys. Lett.* **2000**, 318, 370–378.
- (80) Schütz, M. Low-order scaling local electron correlation methods. III. Linear scaling local perturbative triples correction (T). *J. Chem. Phys.* **2000**, *113*, 9986–10001.
- (81) Schütz, M.; Werner, H.-J. Low-order scaling local electron correlation methods. IV. Linear scaling local coupled-cluster (LCCSD). J. Chem. Phys. 2001, 114, 661–681.
- (82) Schütz, M. Low-order scaling local electron correlation methods. V. Connected triples beyond (T): Linear scaling local CCSDT-1b. *J. Chem. Phys.* **2002**, *116*, 8772–8785.
- (83) Mata, R. A.; Werner, H.-J. Local correlation methods with a natural localized molecular orbital basis. *Mol. Phys.* **2007**, *105*, 2753–2761
- (84) Taube, A. G.; Bartlett, R. J. Frozen natural orbital coupled-cluster theory: Forces and application to decomposition of nitroethane. *J. Chem. Phys.* **2008**, *128*, 164101.
- (85) Li, W.; Piecuch, P.; Gour, J. R.; Li, S. Local correlation calculations using standard and renormalized coupled-cluster approaches. *J. Chem. Phys.* **2009**, *131*, 114109.
- (86) Neese, F.; Hansen, A.; Liakos, D. G. Efficient and accurate approximations to the local coupled cluster singles doubles method using a truncated pair natural orbital basis. *J. Chem. Phys.* **2009**, *131*, No. 064103.
- (87) Neese, F.; Wennmohs, F.; Hansen, A. Efficient and accurate local approximations to coupled-electron pair approaches: An attempt to revive the pair natural orbital method. *J. Chem. Phys.* **2009**, *130*, 114108.
- (88) Piecuch, P. Active-space coupled-cluster methods. *Mol. Phys.* **2010**, *108*, 2987–3015.
- (89) Li, W.; Piecuch, P. Improved Design of Orbital Domains within the Cluster-in-Molecule Local Correlation Framework: Single-Environment Cluster-in-Molecule Ansatz and Its Application to Local Coupled-Cluster Approach with Singles and Doubles. *J. Phys. Chem. A* 2010, 114, 8644–8657.
- (90) Liakos, D. G.; Hansen, A.; Neese, F. Weak Molecular Interactions with Parellel Implementations of the Local Pair Natural Orbital Coupled Pair and Coupled Cluster Methods. *J. Chem. Theory Comput.* **2011**, *7*, 76–87.
- (91) Tew, D. P.; Helmich, B.; Hättig, C. Local explicitly correlated second-order Møller-Plesset perturbation theory with pair natural orbtials. *J. Chem. Phys.* **2011**, *135*, No. 074107.
- (92) Yang, J.; Kurashige, Y.; Manby, F. R.; Chan, G. K. L. Tensor factorizations of local second-order Møller-Plesset theory. *J. Chem. Phys.* **2011**, *134*, No. 044123.
- (93) Yang, J.; Chan, G. K.-L.; Manby, F. R.; Schütz, M.; Werner, H.-J. The orbital-specific-virtual local coupled cluster singles and doubles method. *J. Chem. Phys.* **2012**, *136*, 144105.
- (94) Liakos, D. G.; Neese, F. Improved correlation energy extrapolation schemes based on local pair natural orbital methods. *J. Phys. Chem. A* **2012**, *116*, 4801–4816.
- (95) Hättig, C.; Tew, D. P.; Helmich, B. Local explicitly correlated second- and third-order Møller-Plesset perturbation theory with pair natual orbitals. *J. Chem. Phys.* **2012**, *136*, 204105.
- (96) Riplinger, C.; Neese, F. An efficient and near linear scaling pair natural orbital based local coupled cluster method. *J. Chem. Phys.* **2013**, *138*, No. 034106.

- (97) Krause, C.; Werner, H.-J. Comparison of explicitly correlated local coupled-cluster methods with various choices of virtual orbitals. *Phys. Chem. Phys.* **2012**, *14*, 7591–7604.
- (98) Masur, O.; Usvyat, D.; Schütz, M. Efficient and accurate treatment of weak pairs in local CCSD(T) calculations. *J. Chem. Phys.* **2013**, *139*, 164116.
- (99) Pavošević, F.; Neese, F.; Valeev, E. F. Geminal-spanning orbitals make explicitly correlated reduced-scaling coupled-cluster methods robust, yet simple. *J. Chem. Phys.* **2014**, *141*, No. 054106.
- (100) Werner, H.-J.; Knizia, G.; Krause, C.; Schwilk, M.; Dornbach, M. Scalable Electron Correlation Methods I.: PNO-LMP2 with Linear Scaling in the Molecular Size and Near-Inverse-Linear Scaling in the Number of Processors. *J. Chem. Theory Comput* **2015**, *11*, 484–507.
- (101) Pavošević, F.; Pinski, P.; Riplinger, C.; Neese, F.; Valeev, E. F. SparseMaps-A systematic infrastructure for reduced-scaling electronic structure methods. IV. Linear-scaling second-order explicitly correlated energy with pair natural orbitals. *J. Chem. Phys.* **2016**, *144*, 144109.
- (102) Ma, Q.; Schwilk, M.; Köppl, C.; Werner, H.-J. Scalable Electron Correlation Methods. 4. Parallel Explicitly Correlated Local Coupled Cluster with Pair Natural Orbitals (PNO-LCCSD-F12). *J. Chem. Theory Comput.* **2017**, *13*, 4871–4896.
- (103) Pavošević, F.; Peng, C.; Pinski, P.; Riplinger, C.; Neese, F.; Valeev, E. F. SparseMaps—A systematic infrastructure for reduced scaling electronic structure methods. V. Linear scaling explicitly correlated coupled-cluster method with pair natural orbitals. *J. Chem. Phys.* 2017, 146, 174108.
- (104) Datta, D.; Kossmann, S.; Neese, F. Analytic energy derivatives for the calculation of the first-order molecular properties using the domain-based local pair-natural orbital coupled-cluster theory. *J. Chem. Phys.* **2016**, *145*, 114101.
- (105) McAlexander, H. R.; Crawford, T. D. A Comparison of Three Approaches to the Reduced-Scaling Coupled Cluster Treatment of Non-Resonant Molecular Response Properties. *J. Chem. Theory Comput.* **2016**, *12*, 209–222.
- (106) Kumar, A.; Crawford, T. D. Frozen virtual natural orbitals for coupled-cluster linear-response theory. *J. Phys. Chem. A* **2017**, *121*, 708–716.
- (107) D'Cunha, R.; Crawford, T. D. PNO++: Perturbed Pair Natural Orbitals for Coupled Cluster Linear Response Theory. *J. Chem. Theory Comput.* **2021**, *17*, 290–301.
- (108) D'Cunha, R.; Crawford, T. D. Applications of a perturbation-aware local correlation method to coupled cluster linear response properties. *Mol. Phys.* **2023**, *121*, No. e2112627.
- (109) Pulay, P. Localizability of dynamic electron correlation. *Chem. Phys. Lett.* **1983**, *100*, 151–154.
- (110) Sæbø, S.; Pulay, P. Local configuration interaction: An efficient approach for larger molecules. *Chem. Phys. Lett.* **1985**, *113*, 13–18.
- (111) Saebø, S.; Pulay, P. Fourth-order Møller-Plessett perturbation theory in the local correlation treatment. I. Method. *J. Chem. Phys.* **1987**, *86*, 914–922.
- (112) Neese, F.; Hansen, A.; Liakos, D. G. Efficient and accurate approximations to the local coupled cluster singles doubles method using a truncated pair natural orbital basis. *J. Chem. Phys.* **2009**, *131*, No. 064103.
- (113) Butcher, J. C. A history of Runge-Kutta methods. *Appl. Numer. Math.* **1996**, 20, 247–260.
- (114) Rosenfeld, L. Quantenmechanische Theorie der naturlichen optischen Aktivitaet von Fluessigkeiten und Gasen. Z. Phys. 1929, 52, 161–174.
- (115) Pipek, J.; Mezey, P. G. A fast intrinsic localization procedure applicable for ab initio and semiempirical linear combination of atomic orbital wave functions. *J. Chem. Phys.* **1989**, *90*, 4916–4926.
- (116) Boys, S. F. Construction of Some Molecular Orbitals to Be Approximately Invariant for Changes from One Molecule to Another. *Rev. Mod. Phys.* **1960**, *32*, 296–299.
- (117) Boughton, J. W.; Pulay, P. Comparison of the Boys and Pipek-Mezey Localizations in the Local Correlation Approach and

- Automatic Virtual Basis Selection. J. Comput. Chem. 1993, 14, 736-740.
- (118) Kodrycka, M.; Crawford, T. Local Correlation for Quadratic Coupled Cluster Response Properties. 2023, in preparation.
- (119) Dunning, T. H. Gaussian basis sets for use in correlated molecular calculations. I. The atoms boron through neon and hydrogen. *J. Chem. Phys.* **1989**, *90*, 1007–1023.
- (120) Woon, D. E.; Dunning, T. H. J. Gaussian Basis Sets for Use in Correlated Molecular Calculations. IV. Calculation of Static Electrical Response Properties. *J. Chem. Phys.* **1994**, *100*, 2975–2988.
- (121) Hampel, C.; Werner, H. J. Local treatment of electron correlation in coupled cluster theory. *J. Chem. Phys.* **1996**, *104*, 6286–6297.
- (122) Crawford, T. D.; King, R. A. Locally Correlated Equation-of-Motion Coupled Cluster Theory for the Excited States of Large Molecules. *Chem. Phys. Lett.* **2002**, *366*, 611–622.
- (123) Virtanen, P.; Gommers, R.; Oliphant, T. E.; Haberland, M.; Reddy, T.; Cournapeau, D.; Burovski, E.; Peterson, P.; Weckesser, W.; Bright, J.; et al. SciPy 1. 0: fundamental algorithms for scientific computing in Python. *Nat. Methods* **2020**, *17*, 261–272.
- (124) Crawford, T.; Peyton, B. G.; Wang, Z. *PyCC*. https://github.com/CrawfordGroup/pycc.
- (125) Harris, C. R.; Millman, K. J.; van der Walt, S. J.; Gommers, R.; Virtanen, P.; Cournapeau, D.; Wieser, E.; Taylor, J.; Berg, S.; Smith, N. J.; et al. Array programming with NumPy. *Nature* **2020**, 585, 357–362
- (126) Smith, D. G. A.; Burns, L. A.; Simmonett, A. C.; Parrish, R. M.; Schieber, M. C.; Galvelis, R.; Kraus, P.; Kruse, H.; Di Remigio, R.; Alenaizan, A.; et al. Psi4 1.4: Open-source software for high-throughput quantum chemistry. *J. Chem. Phys.* **2020**, *152*, 184108.
- (127) Smith, D. G. A.; Gray, J. opt_einsum A Python package for optimizing contraction order for einsum-like expressions. *J. Open Source Software* **2018**, *3*, 753.